Space Weather

RESEARCH ARTICLE
10.1029/2025SW004629

The MANA Magnetometer Array, and Magnetic Observations Across New Zealand From 2024

John Malone-Leigh[1], Craig J. Rodger[1], Aaron T. Hendry[2], James Brundell[1], Daniel Mac Manus[1], Tanja Petersen[3], Lisa Evans[1], Mikhail Kruglyakov[1], and Xinhu Feng[1]

[1]Department of Physics, University of Otago, Dunedin, New Zealand, [2]British Antarctic Survey, Cambridge, UK, [3]Earth Sciences New Zealand, Data Science and Geohazards Monitoring, Lower Hutt, New Zealand

Abstract This paper describes the Magnetometer Array for New Zealand Aotearoa, or MANA, completed in 2023. The network consists of five new variometer sites to complement the existing Eyrewell geomagnetic observatory. Here, we describe the technical details and capabilities of the network, including the hardware and software used. Data products include the standard 1 s cadence magnetic field time series (and up to 130 Hz upon request), as well as the MANA website used to monitor geomagnetic storms (https://solartsunamis.otago.ac.nz/mana/data/). We also report on observations from the MANA network as an example of the network operating, specifically from the 10–12 May and 10–12 October 2024 geomagnetic storms. The 10–12 May 2024 "Gannon" storm was the largest geomagnetic storm observed in New Zealand since 1994, and hence is of particular interest, with a maximum recorded $\frac{d\mathbf{H}}{dt}$ of 478 nT/min at Awarua and 321 nT/min at Eyrewell (exceeding the previous maximum of 191 nT/min in November 2001). The 10–12 October geomagnetic storm was a smaller event, with more variable magnetic field observations across New Zealand and was the fifth largest since 1994 in terms of $\frac{d\mathbf{H}}{dt}$. This storm had a maximum recorded $\frac{d\mathbf{H}}{dt}$ of 202 nT/min at Awarua, while simultaneously, a $\frac{d\mathbf{H}}{dt}$ spike of only 40 nT/min was observed at Eyrewell. The local maxima for each of these storms occurred roughly 10 hr after the global maxima. Significant differences between the local H30- and global Hpo-indices indicated that localized phenomena were driving these events, most likely substorms.

Plain Language Summary Disturbances of Earth's magnetic field lead to the generation of geomagnetically induced currents (GICs) in infrastructure like power grids, which can cause damage and even power grid blackouts in some extreme cases. Thus, observations of the magnetic field are of practical importance. The Magnetometer Array for New Zealand Aotearoa (MANA) magnetometer array, set up to monitor these disturbances in New Zealand, is described. The network is made up of five magnetometers, devices that measure the Earth's magnetic field. An explanation of how the network operates is given. It collects magnetic field data every second, and even faster if needed. These data are also live plotted on the MANA website (https://solartsunamis.otago.ac.nz/mana/data/). The paper shares examples of two very significant geomagnetic storms recorded in 2024. The first, in May, was the biggest storm in New Zealand since 1994, in terms of the rate of change of **H**, the magnetic field strength that points toward geomagnetic north. The second, in October, was the fifth largest storm since 1994. These storms peaked in New Zealand about 10 hr after the biggest global peaks, showing that local factors influenced what happened. These local factors were likely due to substorms, a magnetic field disturbance related to the night side of the Earth.

Key Points:

- A new network of five variometer sites across New Zealand, Magnetometer Array for New Zealand Aotearoa, is outlined, including technical details of the network
- The May "Gannon" 2024 storm was the largest storm in terms of horizontal rate of change of the magnetic field since 1994 (max 478 nT/min)
- The October 2024 storm was weaker, though relatively large (max 202 nT/min)

Correspondence to:
J. Malone-Leigh,
john.m.leigh@otago.ac.nz

Citation:
Malone-Leigh, J., Rodger, C. J., Hendry, A. T., Brundell, J., Mac Manus, D., Petersen, T., et al. (2026). The MANA magnetometer array, and magnetic observations across New Zealand from 2024. *Space Weather*, *24*, e2025SW004629. https://doi.org/10.1029/2025SW004629

Received 17 JUL 2025
Accepted 4 OCT 2025

Author Contributions:
Conceptualization: John Malone-Leigh, Craig J. Rodger, Aaron T. Hendry, James Brundell
Data curation: John Malone-Leigh, Aaron T. Hendry, Tanja Petersen
Formal analysis: John Malone-Leigh, Craig J. Rodger, Aaron T. Hendry
Funding acquisition: Craig J. Rodger
Investigation: John Malone-Leigh, Craig J. Rodger, Daniel Mac Manus
Methodology: John Malone-Leigh, Craig J. Rodger, Aaron T. Hendry, James Brundell, Daniel Mac Manus, Tanja Petersen
Project administration: Craig J. Rodger
Resources: John Malone-Leigh, Aaron T. Hendry, James Brundell, Tanja Petersen, Xinhu Feng
Software: John Malone-Leigh, Aaron T. Hendry, Lisa Evans
Supervision: Craig J. Rodger

1. Introduction

Ground-based magnetometers are a highly effective tool, used globally to investigate geomagnetic disturbances. Magnetometers measure the sum of magnetic fields generated by currents flowing outside of the Earth, that is in the magnetosphere and ionosphere, and those generated internally due to electromagnetic induction in the Earth. The magnetic field variations generated by these currents can be used to understand the ground-based impact of geomagnetic disturbances originating from impacts by solar storms.

In New Zealand (NZ), a single magnetometer has been used to measure the impact of geomagnetic storms, the Eyrewell INTERMAGNET observatory, operated by Earth Sciences New Zealand (formerly GNS Science). The Eyrewell observatory has existed since 1978, with accurate digital recordings since 1990 (although only records from 1994 onward are currently disclosed). While a single magnetometer is useful for quantifying local magnetic field conditions, previous studies have demonstrated that a higher density of magnetometers is required to

Validation: John Malone-Leigh, Craig J. Rodger, Aaron T. Hendry, James Brundell, Daniel Mac Manus, Mikhail Kruglyakov
Visualization: John Malone-Leigh
Writing – original draft: John Malone-Leigh
Writing – review & editing: Craig J. Rodger, James Brundell, Daniel Mac Manus, Tanja Petersen, Lisa Evans, Mikhail Kruglyakov, Xinhu Feng

accurately reproduce geomagnetic storm effects at ground level. A density of roughly 200 km is required to accurately replicate the regional magnetic field variation at mid-latitude required for geomagnetically induced current (GIC) modeling (Campanyà et al., 2019; Malone-Leigh et al., 2023; McLay & Beggan, 2010), while a denser grid of 50–100 km is required to replicate more spatially and temporally localized magnetic field variations, generally related to the auroral electrojet, which occur at higher latitudes (Belakhovsky et al., 2019; Juusola et al., 2016). With all this in mind, a new magnetometer array, the Magnetometer Array for New Zealand Aotearoa (MANA) was established to complement the Eyrewell observatory. Each site was installed approximately equidistant across New Zealand at approximately this 200 km separation for mid-latitudes. MANA is similar to many other magnetometer networks, such as IMAGE in Fennoscandia, CARISMA in Canada and the United States, and Stel in Japan (Mann et al., 2008; Shiokawa et al., 2010; Tanskanen, 2009). The goal of this network was to more accurately replicate localized effects during these storms in order to improve GIC modeling in the New Zealand power grid. Later in this manuscript, the technical details of the MANA network will be outlined.

It is generally accepted that the main threat posed by geomagnetic storms to electrical power transmission networks is GIC (United Nations, 2017). During geomagnetic storms, a complex interaction between magnetic field variations and the underlying electrical conductivity structure of the uppermost layer of the Earth, the lithosphere, generates electric fields at the surface (Tikhonov, 1950). These electric fields, in turn, drive geomagnetically induced currents in ground-based infrastructure such as power grids, pipelines, railways, and historically impacted telegraph lines also (Boteler, 2006; Divett et al., 2023; Mac Manus et al., 2017; Patterson et al., 2024). GIC can adversely affect these infrastructure in multiple ways, through physical damage and disruption of services, with the potential to cause billions of dollars in losses to the economy on a national scale. For example, Oughton et al. (2019) estimates a loss in gross domestic product of £15.9 billion due to a 1-in-100-year geomagnetic storm in the United Kingdom (UK). The main aim of setting up the MANA network is to have an increased density of magnetometers to help model and understand GIC across NZ.

An especially high density of GIC measurements is present in NZ, thanks to the work by Transpower NZ. The NZ power grid is also isolated from other power networks, making it an ideal location to study the impact of geomagnetic storms on power networks. Previous modeling and observations have demonstrated that NZ is vulnerable to geomagnetic storms. Béland and Small (2005), reported that a large GIC induced during the November 2001 geomagnetic storm caused the destruction of a power system transformer at Halfway Bush, Dunedin and caused tripping in two sets of voltage control equipment on the South Island. Mac Manus et al. (2017) reports that the large GIC originated from a large magnetic field variation, 191 nT/min, caused by the arrival of a sudden commencement (SC). Rodger et al. (2017, 2020) demonstrated that rapid variations of the horizontal component of the magnetic field, during geomagnetic storms, were more likely to drive large GICs. Smith et al. (2024) showed this to be particularly true in NZ for SCs related to the impact of coronal mass ejections. Mac Manus et al. (2017, 2022) has modeled the impact that a geomagnetic storm would have on the NZ power grid, identifying regions of the grid particularly susceptible to large GICs and developing a strategy to help mitigate this (Mac Manus et al., 2023). Most notably, regions in the south of NZ are typically the most susceptible, due to a combination of characteristics, a higher rate of change of the magnetic field, a resistive conductivity structure, and the configuration of the New Zealand power grid (Clilverd et al., 2020; Mac Manus, 2023; Pratscher et al., 2024). However, most of these studies have been somewhat limited by the lack of magnetometer coverage in NZ, as well as the lack of severe geomagnetic storms in the last 20 years, that is, limited numbers with $Kp \geq 8$ (Abe et al., 2023).

In more recent times, two of the largest geomagnetic storms in 20 years occurred, the 10–12 May and 10–12 October 2024 storms. The former is often dubbed the "Gannon storm" after Jennifer Gannon, an influential member of the space weather community, sometimes alternatively called the "Mother's day" storm in recent literature (Lugaz et al., 2024). Here, it will be referred to as the Gannon storm or the May 2024 storm, while with the latter, we simply use the October 2024 storm. The Gannon storm was particularly strong. Elvidge and Themens (2025) estimated the storm to be a roughly 1-in-12.5 year event in terms of amplitude and 1-in-40 year event in terms of duration, based on global magnetic indices. In NZ, Mac Manus et al. (2025) reported on GIC observations from the Gannon storm with a maximum GIC measured of 113 A (although a value of 200 A was expected had the mitigation plan not been enacted), Clilverd et al. (2025) reported on harmonics and reactive power observed in the grid, while Ingham et al. (2025) reports on effects in the NZ gas pipeline network. GIC in excess of 30 A were also reported in many other regions of the world and/or large modeled geoelectric fields in

excess of 0.5 V/km, including the UK, Canada, Finland, Sweden, and China (Cordell et al., 2025; Lawrence et al., 2025; Piersanti et al., 2025; Rosenqvist et al., 2025; Shao et al., 2024). The installation of the MANA network was completed and fully operational just before these events in early 2024, so these storms offered a perfect opportunity to gauge how variable the magnetic field response is across the entirety of New Zealand.

Here, we describe the newly installed MANA array. This includes instrument specifications, electronic and physical setup at variometer sites, as well as the data acquisition method of the network as a whole. Then, observations from MANA for the May and October 2024 storms will be explored, by analyzing $\frac{d\mathbf{H}}{dt}$, SME/U/L indices and H30-indices.

2. The MANA Magnetometer Array

The Magnetometer Array for New Zealand Aotearoa (MANA) began as part of the Solar Tsunami Endeavour Programme (which we will shorten to "Solar Tsunamis"). Solar Tsunamis is an overarching space weather based project across New Zealand with the objective to study the ground-based effects of geomagnetic storms across New Zealand. The project involves multiple industry and research partners, with the aim of mitigating the hazard posed by GIC to national energy networks. MANA was established with this objective in mind. The acronym MANA conveniently matched the Te Reo Māori word for power and vitality, so it was chosen. The primary aim of MANA is to measure magnetic field time series accurately across New Zealand. These time series can then be used as inputs to model the geomagnetic field variations, geoelectric fields and hence improve GIC modeling across New Zealand, both for real-time applications and in retrospect.

The new MANA array consists of five variometer sites installed throughout New Zealand to complement Eyrewell. These sites use 3-axis fluxgate magnetometers. Two of these sites were installed on the North Island, two on the South Island and one to the far east on the Chatham Islands (Figure 1, Table 1). Each of these sites were chosen strategically: Donnelly and Awarua are located in the northern- and southern-most points of NZ, Swampy is near the site of the largest predicted GIC in NZ and previous transformer damage (Mac Manus et al., 2022), Oakview is near the largest gas pipeline in the country (Ingham et al., 2022), while the Chathams give us a point far to the east, which can improve the magnetic field interpolation (other INTERMAGNET sites exist to the south, west, and north of New Zealand). The mainland variometers were also installed approximately along the same magnetic longitudinal meridian (Figure 1). The network is one of the densest of its kind in the Southern Hemisphere and is in a region with minimal coverage of magnetic field measurements from a global perspective. Below, the technical aspects of this network are described in Sections 2.1 and 2.2.

2.1. Equipment

The physical aspects of the variometer sites, that is, the magnetometer equipment, design of the chamber, and the electronic set-up used are described in this section. The goal when constructing the magnetometer setup was to build a network which could provide high-quality data sufficient for space weather, though in a non-invasive, cheaper and simpler manner than a typical geomagnetic observatory, which can require extensive regular tasks. Most of the sites are generously hosted on private property some distance from the research groups' home base. Thus, simplicity in the physical installation was prioritized.

2.1.1. The Magnetometer and Electronic Setup

The main magnetometer used for the network is the Bartington Instruments Mag-13 3-axis fluxgate. It is a high-quality magnetometer suitable for space weather, although cheaper than the observatory grade (Figure 3). An equivalent but older Bartington Mag-03 3-axis fluxgate is used at Swampy. At the INTERMAGNET site in Eyrewell, an observatory grade 3-axis fluxgate from the Technical University of Denmark (DTU) is used (Pedersen & Merenyi, 2016). The specifications for these magnetometers are provided in Table 2, the main difference between the Mag-13 and the FGE being thermal stability. The electronic set-up below is designed in such a way that these magnetometer types could easily be interchanged with others. A schematic of this setup is shown in Figure 2.

A power supply unit (PSU) provided by Bartington is used to filter the power supply and deliver power to the magnetometer. A USBX4CH analog-to-digital converter (ADC) from Symmetric Research is used to acquire data from the magnetometer. This ADC can be used interchangeably for most magnetometers, has software available

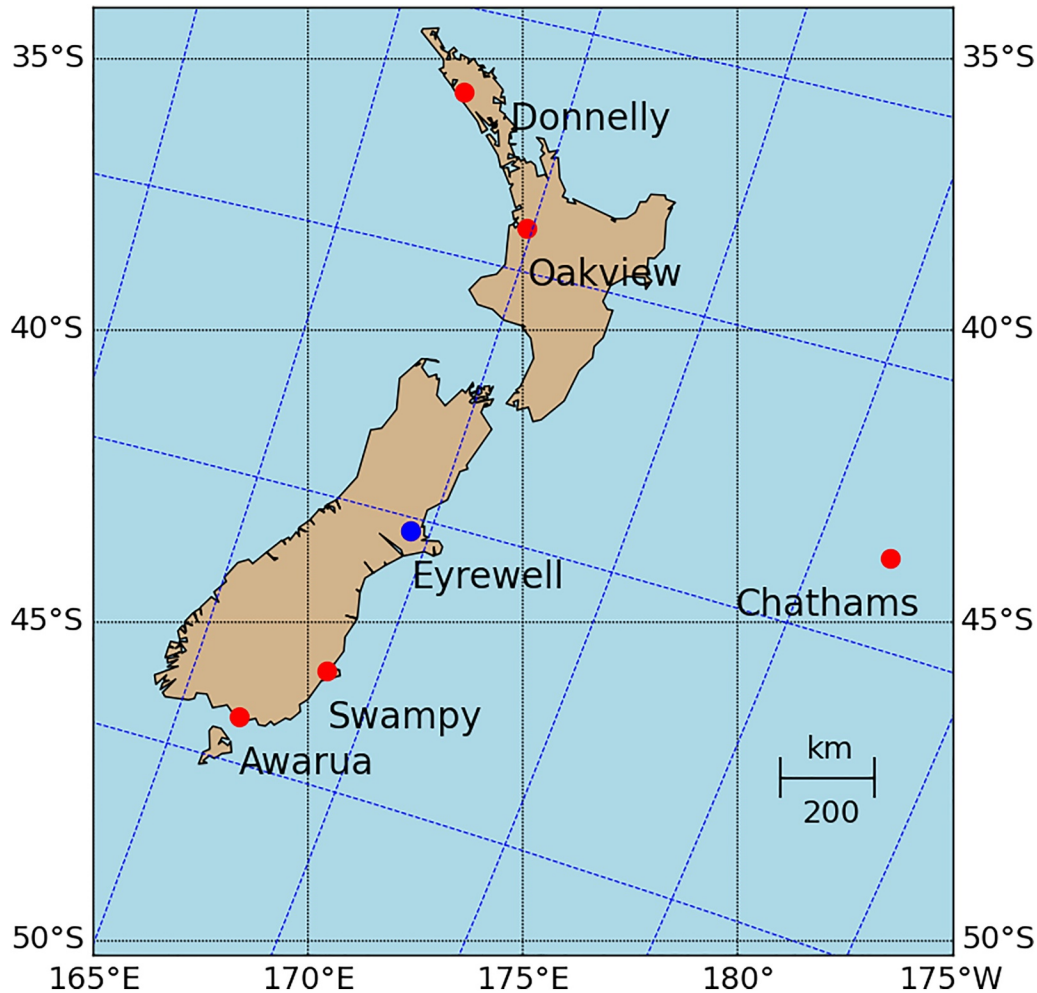

Figure 1. The MANA magnetometer network variometers. The long term existing INTERMAGNET observatory at Eyrewell (blue) is complemented with five new variometer sites (red) across NZ. Blue dashed lines are used to denote the IGRF CGM longitudinal meridians and parallels, while black dashed lines are used for the geodetic meridians and parallels.

for Windows, Linux, and Mac, uses a convenient USB connection, and its sample rate can be easily varied between approximately 1–10,000 Hz. Ideally, a sampling rate of at least 120 Hz should be used (Morschhauser et al., 2017). Specifically, this allows for sufficient reconstruction and hence removal of noise from power lines at 50 Hz, to satisfy the Nyquist criterion. In our case, we chose a sampling rate of approximately 130 Hz on the ADC.

Table 1
The Location of the MANA Sites and Eyrewell in Geodetic and Corrected Geomagnetic (CGM) Coordinates, Calculated Using the IGRF Magnetic Field Model With https://omniweb.gsfc.nasa.gov/vitmo/cgm.html

Site	Geodetic Lon (°E)	Geodetic Lat (°S)	CGM Lon (°E)	CGM Lat (°S)	Install date	Magnetometer
Awarua	168.39	46.53	254.68	54.04	October 2021	Mag-13
Chathams	183.47	43.94	269.65	48.30	August 2022	Mag-13
Eyrewell	172.39	43.47	257.45	50.10	January 1978	DTU FGE
Donnelly	173.64	35.62	255.22	41.73	March 2023	Mag-13
Oakview	175.10	38.16	257.85	44.09	May 2022	Mag-13
Swampy	170.48	45.79	256.63	52.87	September 2016	Mag-03

Note. The dates of first installation and the type of magnetometer for each site are also included.

Table 2
The Specifications of the Bartington Mag-03, Mag-13, and DTU 3-Axis FGE Set Up Used at Each Observatory

Device	Dynamic range (nT)	Resolution (nT)	Thermal drift (nT/°C)	RMS noise ($1/\sqrt{\text{Hz}}$ @1 Hz)	Sample rate (Hz)
Mag-03/-13	±70,000	0.01	<0.6	<6 pT	130.2083
DTU FGE	±3,200	0.01	<0.25	35 pT	1.0

Note that the Eyrewell site is instead equipped with a DTU electromagnetic compatibility board, which filters this noise via hardware rather than software. The ADC is connected to a GPS unit and uses this for data timing. The ADC transmits data to a Raspberry Pi computer (RPi) operating Raspberry Pi OS.

Powering variometer sites can be a challenge, as quiet locations are ideally required to be away from man-made noise sources such as cars and power lines, which magnetometers are sensitive to (Schmidt et al., 2020). Unfortunately, power sources are often found in these areas with noise. Hence, in terms of providing power for the equipment, two approaches were taken:

1. At sites where mains electricity is readily available and noise is low, power was simply delivered through an ethernet cable via power over ethernet, PoE (i.e., within roughly 50 m of a mains outlet). A PoE injector was used to add power to the router's ethernet cable. A PoE splitter was used to transfer back into power and communications.
2. At the more remote Awarua and Donnelly sites, no noise-free power source was available. Hence, solar panels and batteries were used instead. Design b was inspired by the variometer design of Hübert et al. (2020). Three 100 Ahr lead-acid batteries are connected in parallel and are used to store power at each site. At Donnelly, a single 170 W solar panel supplies power to the magnetometer, while two of these, totaling 340 W, are present at Awarua in the south to ensure sufficient power is delivered. A solar charge controller, the SmartSolar Charge Controller from Vitron Energy, manages the power transfer between the batteries, solar panels, and equipment.

In total, the MANA variometer set-up uses ≤12 W on average. Thus, only a few hours of sunlight are required daily to power the equipment. 300 Ahr batteries store 3,600 Whr in total. Hence, the system can theoretically

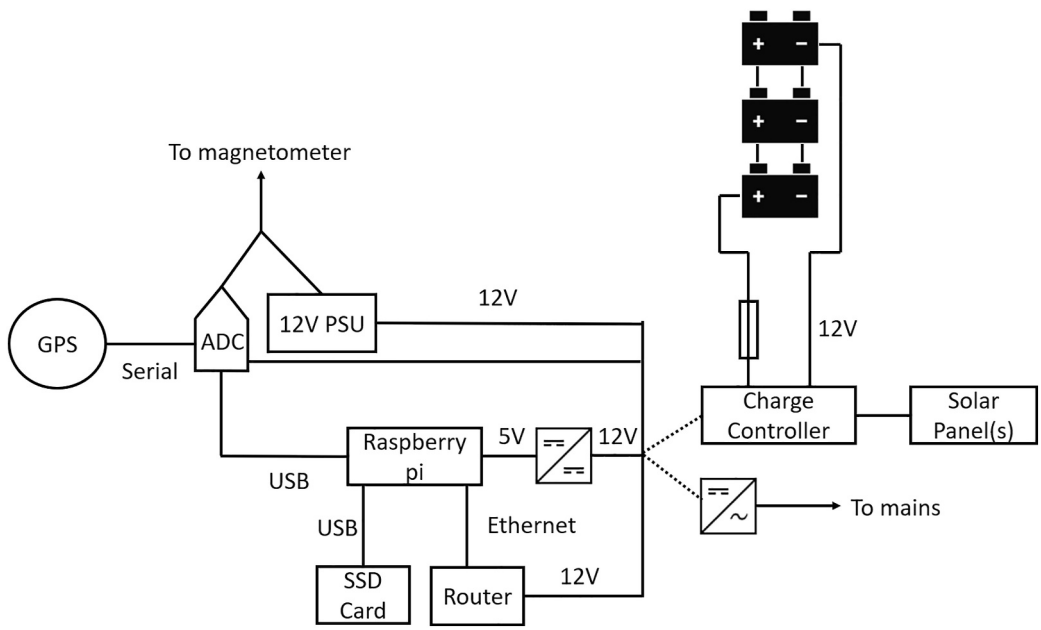

Figure 2. A schematic diagram of the magnetometer wiring setup. A RPi and router are used for data acquisition and transmission. An ADC reads data from the magnetometer, and transmits back to the RPi, with a GPS used to keep the time. A custom power supply unit with a filter is used to supply the power to the magnetometer. Depending on the site, either (a) mains power or (b) solar panels with batteries, are used to supply the power.

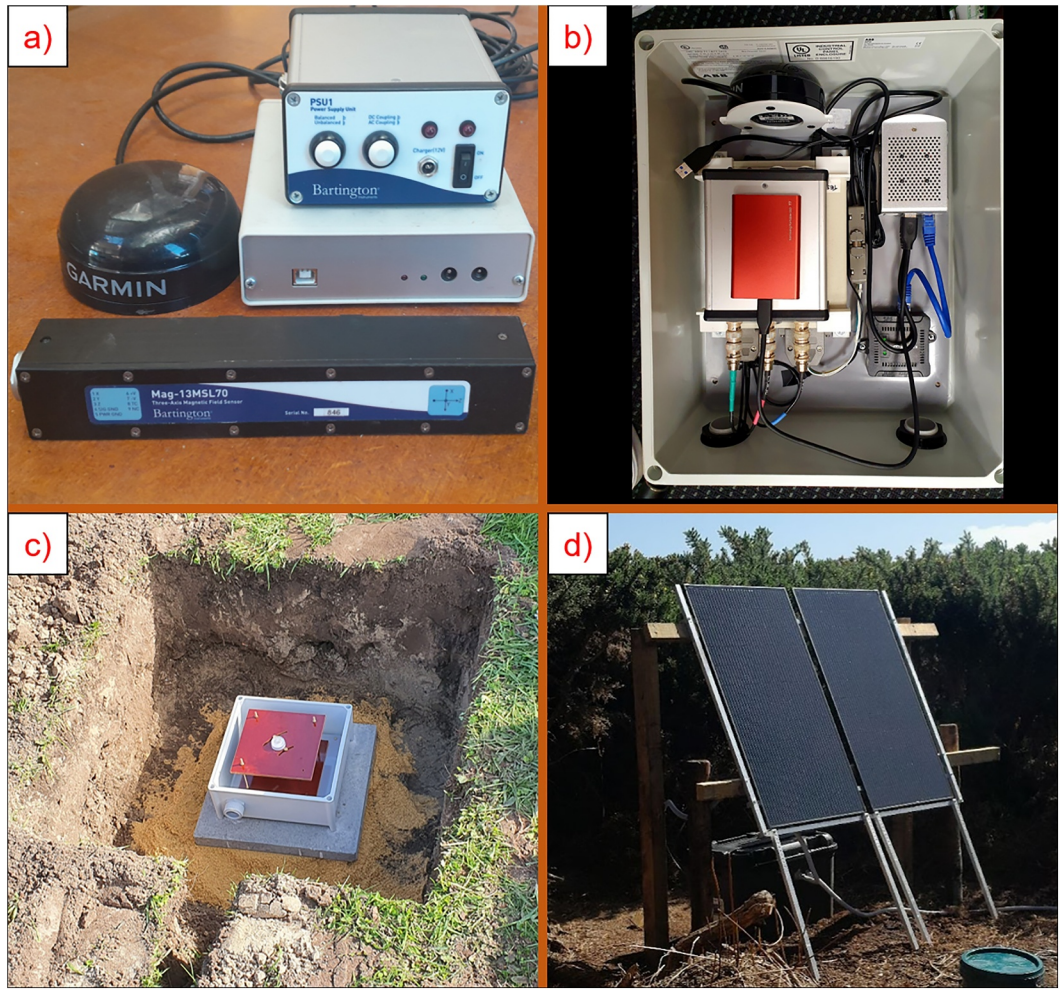

Figure 3. (a) Equipment used at the sites, including the Mag-13 at the front, the GPS unit on the left and the PSU atop the ADC on the right. (b) An example of the data logger box. The RPi was stored in a protective metal box (top-right), while a POE splitter brings power and ethernet to the setup. (c) A magnetometer chamber atop a concrete slab with the Tufnol baseplate inside pre-burial. (d) The solar panel setup of the Awarua magnetometer, with a larger data logger box below the panels. In this case, the solar panels were oriented to 60°N to ensure optimal solar charging in the winter months.

operate for 300 hr, or 12.5 days without any sunlight (3,600 Whr/12 W). In reality, only 75% of this can be used to avoid damaging the batteries, so the system can last 225 hr or 9.4 days. This power storage is critical during the winter months, when cloudy weather is more common.

A schematic of the electronics for both designs is shown in Figure 2.

2.1.2. Variometer Installation

Observatory grade magnetometers are generally installed above ground on plinths or below ground in concrete vaults, which are sheltered from the elements and heat regulated to reduce thermal noise. However, this type of installation is expensive and is not suitable for temporary installations. The alternative approach which can be used to reduce thermal noise is instead to bury the magnetometer in a chamber. The majority of MANA magnetometers were buried, the exception being Swampy, as a plinth was already available at this site (though not heat-regulated). Although not sufficient for absolute measurements, these sites can be used for magnetic field variations and are more often referred to as variometers to distinguish them from geomagnetic observatories. The variometers were buried approximately 50 cm deep. The magnetometer chamber is used to house the magnetometer. The chamber was cemented in place using a non-ferrous concrete mixture where possible, or was placed on a concrete slab instead. Inside the chamber, the magnetometer was oriented to geodetic north, that is XYZ

coordinates calculated using IGRF-14 (Alken et al., 2021). The magnetometer is fastened to a Tufnol base-plate using brass bolts. The equipment and chamber installation is shown in Figure 3.

2.2. Data Acquisition, Processing, and Availability

A series of C++ programs and shell scripts were developed to acquire the variometer data from the ADC in real time. C++ programs are first used for serial communications between the Raspberry Pi and the ADC. These C++ programs read 130 Hz binary packets from the ADC and save these data locally on a solid-state drive (SSD) connected to the RPi. A combination of C++ programs and shell scripts are then used to calibrate the magnetic field input, correctly timestamp, and archive these data locally. Finally, C++ programs controlling Unix sockets were used to automatically transmit individual data packages in real time, via a reverse shh tunnel over the router to a storage server, where all the magnetometer data were housed. The scp and rsync functions were later used to update the files and include any packets that were missed. Much of this is similar to the method of Morschhauser et al. (2017).

A Python script is used to process and plot the data, both locally and on the storage server. Data are downsampled from 130 to 1 Hz, with a low-pass filter applied at frequencies higher than 2 Hz to remove any noise in this range, within INTERMAGNET specifications. 1 Hz is usually sufficient to replicate the GIC time series accurately (Hartinger et al., 2023; Heyns et al., 2021; Trichtchenko, 2021). Hence, this is the standard output in which we provide our time series. However, the measured 130 Hz can allow for investigation of phenomena that require a shorter temporal resolution, that is PC1 waves, Pib pulsations, and electromagnetic ion cyclotron waves in the magnetosphere (Hendry et al., 2016; Obana et al., 2024). Saving these 130 Hz data allows for the option to later revisit events at a shorter cadence, where necessary.

In real time, a simple peak-finding algorithm is employed to identify large noise spikes: (a) spikes above 10–25 nT/s in one-second cadence data are marked (amplitude is site dependent), (b) if an unusual noise-like spike is identified at only one site, it is flagged and a one minute window of data around that spike is temporarily removed (between 0–59 s), (c) if a peak is simultaneously observed at two sites within the same one minute window, it is again flagged, however no data is removed from the time series. Later, the team can manually confirm if the peaks are due to noise. The live data are then plotted on the MANA website (https://solartsunamis.otago.ac.nz/mana/data/). Data are distributed upon request by the University of Otago, Space Physics Group, at this 1 Hz sampling rate, or where applicable the native 130 Hz rate.

3. Quantifying Magnetic Activity

3.1. Magnetic Variability

Quantifying geomagnetic storms is often performed by examining the peaks and duration of strong activity in $\mathbf{H}$, the horizontal component of the magnetic field, and its rate of change $\frac{d\mathbf{H}}{dt}$ at a temporal resolution of 1 minute (e.g., Dimmock et al., 2020; Thomson et al., 2011; Viljanen et al., 2001). GICs are ultimately induced by the interaction between the temporal change of the magnetic field with the conductive Earth, with the horizontal component particularly likely to induce a GIC due to its relative orientation parallel to the surface (Pirjola, 2002; Viljanen, 1998).

The INTERMAGNET Gaussian-weighted digital filter was used to filter and bin the data from 1-s to 1-min temporal resolution, to allow consistency in the comparison between measurements. This involves multiplying the 1-s time series by filter coefficients centered on the minute and taking the sum of these values over the entire minute to output 1-min data (Love & Chulliat, 2013; St-Louis, 2024).

$\mathbf{H}$ and $\frac{d\mathbf{H}}{dt}$, are calculated as follows, using the $\mathbf{X}$ and $\mathbf{Y}$ components of the magnetic field:

$$\mathbf{H} = \sqrt{\mathbf{X}^2 + \mathbf{Y}^2} \tag{1}$$

$$\frac{d\mathbf{H}}{dt} = \frac{\sqrt{[\mathbf{X}(t+dt) - \mathbf{X}(t)]^2 + [\mathbf{Y}(t+dt) - \mathbf{Y}(t)]^2}}{dt} \tag{2}$$

Note that the rate of change used is the displacement of **H**, previously used by Viljanen et al. (2001); Smith et al. (2019). Some other studies use the rate of change of the magnitude of **H**, such as Thomson et al. (2011). Currently, **H** and $\frac{d\mathbf{H}}{dt}$ are used to monitor geomagnetic activity across New Zealand (https://solartsunamis.otago.ac.nz/mana/data/). Later in this paper, $\frac{d\mathbf{H}}{dt}$ time series from previous storms were calculated using this method.

3.2. Local H30-Indices

Over longer timescales, the Kennziffer indicator or K-index is traditionally and most often used to quantify activity over longer time spans. The K-index provides three-hour windows of the activity of the local **H**, obtained from magnetometer measurements, with a solar regular curve subtracted. The scale of the *K*-index is quasi-logarithmic and ranges from 0–9, where $K = 0$ indicates completely quiet conditions, $K = 5$ indicates a minor storm and $K = 9$ indicates a severe storm (Bartels et al., 1939; Matzka et al., 2021; Riddick & Stuart, 1984).

Yamazaki et al. (2022) recently introduced an adaptation of K-indices, H30- (and H60-) indices, which mitigate some of the original limitations of K-indices. The temporal resolution of the indices was shortened to 30 min and the upper limit of $K = 9$ was replaced such that there is no upper limit, that is an unbounded limit. When later evaluating the 10–12 May and 10–12 October geomagnetic storms, H30-indices were used to compare the local strength of the storms, alongside $\frac{d\mathbf{H}}{dt}$. Here, we employed this method to produce H30-indices, implementing the Finnish Meteorological method for computing (Menvielle et al., 1995). At Eyrewell, a predefined $K = 9$ threshold of 540 nT, used for *K*-indices, was also used for the H30-indices. An estimate of 750 nT at $K = 9$ was used for Awarua. H30-indices were later compared with the global Hpo-index (Hp30), to contrast local activity with global activity. The H30-indices at other sites were not plotted later, to maintain simplicity for the analysis. Although H30-indices are currently not available on the MANA website, the intention of the group is to use them to monitor, in near real time, the magnitude of local geomagnetic field variations in the future.

3.3. AE and SME Indices

The auroral electrojet (AE) index is used to quantify the activity of a geomagnetic storm in the auroral region (60–75°). The index calculates the maximum difference between the eastward (AU) and westward (AL) ejectrojet in nT across 16 observatories to obtain the AE index (Rostoker, 1972).

In terms of mid-latitude countries, such as New Zealand, the AE index is useful in determining the presence of substorm expansions, which are often associated with the largest magnetic field variations (Fogg et al., 2023; McPherron & Chu, 2017). A largely negative AE indicates a likely substorm expansion.

The SuperMAG electrojet index (SME index) is an updated, though unofficial, version of the AE index (Gjerloev, 2012). It includes all available magnetic field data in the SuperMAG data set, unlike AE which is limited to 16, again calculating the difference between the eastward (SMU) and westward (SML) electrojet. Hence, it is more representative, although it may be subject to bias when certain areas have greater densities of magnetometers (Bergin et al., 2020). We made use of the SME/U/L index later in the manuscript to allow for identification of possible substorm expansions impacting magnetic fields in New Zealand.

4. Observations From the May and October 2024 Storms

In the following sections, observations from the MANA array of the May and October 2024 geomagnetic storms are outlined. In Sections 4.1 and 4.2, the rate of change of the magnetic field is examined and times of interest are defined, that is large spikes in the magnetic field. In Section 4.3, the SME index is compared to these spikes to help determine whether the spikes relate to substorm expansions. Then in Section 4.4, activity in MANA is compared with global activity using H30- and Hp30-indices.

4.1. 10–12 May 2024 Gannon Storm

Significant solar activity preceded the geomagnetic storm on 10–12 May 2024. Active region 12,664 produced numerous M and X class flares between 6–10 May, with at least five corresponding halo CME's observed by SOHO LASCO, indicating a likely impact with Earth (Parker & Linares, 2024). A first ground-based impact was observed at approximately 17 UT on 10 May, with the resulting storm persisting until late on 12 May. Globally,

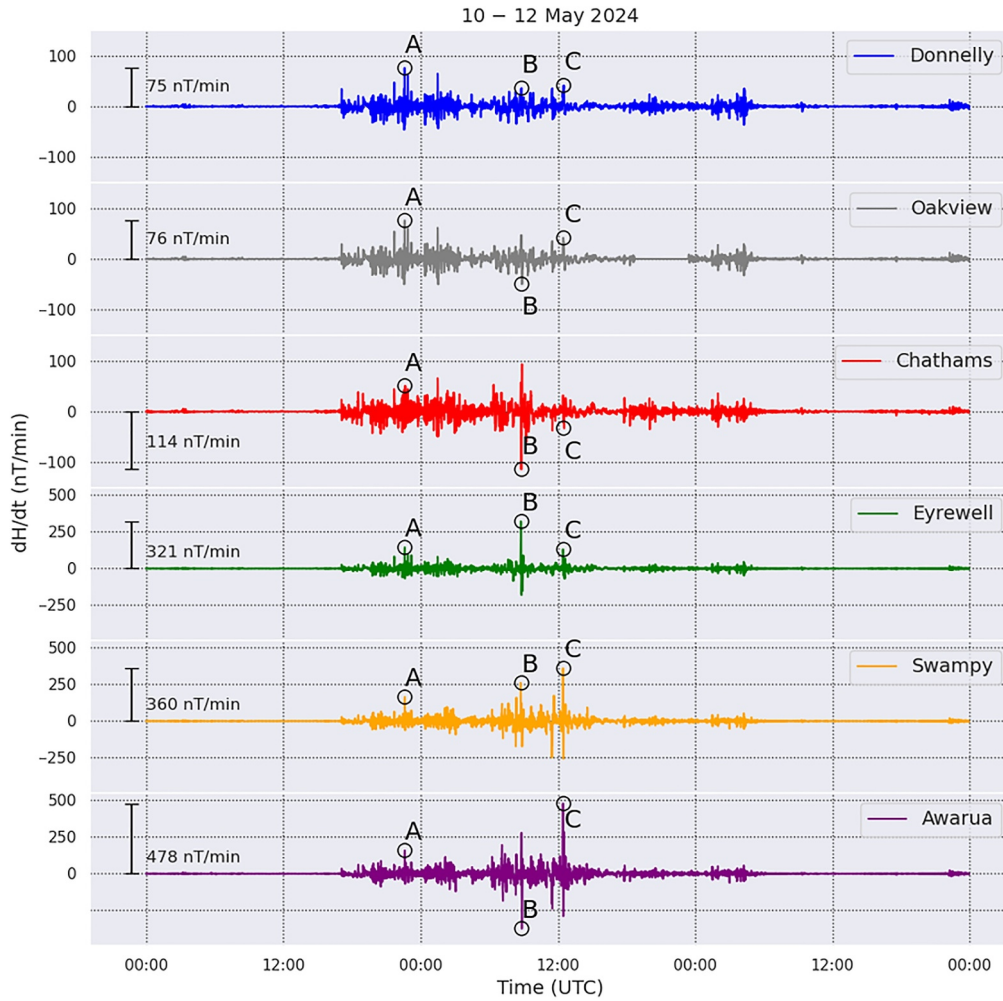

Figure 4. The rate of change of the magnetic field (**H**) during the 10–12 May 2024 geomagnetic storm across the MANA array, arranged from northernmost to southernmost (i.e., equatorward to poleward). Three large spikes denoted by A, B and C were observed at approximately 22:35 UT, 10 May 2024, 08:50 UT, and 12:30 UT, 11 May 2024. An overall peak of 478 nT/min at Awarua was observed for the last of these spikes.

the impact of this storm was the largest observed since the 20–21 November 2003 storm in terms of many magnetic field indices, including Kp and DST (Elvidge & Themens, 2025; Hayakawa et al., 2025).

Here, we focus on the magnetic activity of the geomagnetic storm across New Zealand. Figure 4 displays the $\frac{d\mathbf{H}}{dt}$ observed time series at the MANA sites throughout New Zealand for this storm. In particular, three large spikes in $\frac{d\mathbf{H}}{dt}$ were observed, labeled as A, B, and C in Table 3. Spike A was observed at roughly 22:35 UT on 10 May. Spike A is the weakest of the three, though it is still a relatively large spike compared to other weaker storms outside this time period. Spike A is also the strongest spike in the North Island. Spike A was most likely due to a global enhancement in the ring current (Elvidge & Themens, 2025), which led to a global peak in magnetic field variability, represented by Hpo-indices (also see Section 4.4). Spike B occurred at approximately 08:50 UT on 11 May. Spike B was large in the South Island, though weak in the North Island. It was also the largest spike observed at Eyrewell (320 nT/min), which was unusual given its magnetic latitude relative to Swampy and Awarua (Mlat 50.10° vs. 52.87° and 54.04°). Spike B was likely generated by a substorm expansion based on SME index (see Section 4.3), as well as global observations of the magnetic field from De Michelis and Consolini (2025). Spike C occurred at approximately 12:30 UT on 11 May. A strong change occurs at Eyrewell, Swampy and Awarua with a much weaker impact at the other three sites. Spike C was also the largest during the storm in total, peaking at 478 nT/min at Awarua. This spike was likely generated by another substorm expansion (see Section 4.3).

Table 3
*The Absolute Value of Peaks Observed for the Rate of Change of the Horizontal Magnetic Field, **H**, in Figure 4 During the May 2024 Storm at Each Site*

Site	Spike A 22:35 UT (nT/min)	Spike B 08:50 UT (nT/min)	Spike C 12:30 UT (nT/min)
Donnelly	75	36	41
Oakview	76	50	41
Chathams	51	114	32
Eyrewell	144	321	130
Swampy	164	260	360
Awarua	158	374	478

The magnetic field variation was the largest observed, since 1994 at Eyrewell, in terms of $\frac{d\mathbf{H}}{dt}$ with a maximum of 321 nT/min. A previous high of 191 nT/min was recorded on 6 November 2001. The Gannon storm was also the third largest storm in terms of absolute magnetic field at Eyrewell, $\Delta H \approx 650$ nT, after both Halloween storms, 29–31 October and 20–21 November 2003.

4.2. 10–12 Oct 2024 Geomagnetic Storm

The October geomagnetic storm originated from solar activity associated with AR 3848. On 9 October, two X1, and one M7 class flares occurred with associated halo CME's observed by SOHO LASCO. These three CMEs drove the geomagnetic storm upon their arrival at Earth. Globally, the start of the geomagnetic storm was marked by a considerably large sudden storm commencement (SSC). The storm was the largest global geomagnetic disturbance since the Halloween 2003 storms, with the exception of the aforementioned Gannon storm (Oliveira et al., 2025).

At the MANA variometer sites, three distinguishing spikes in $\frac{d\mathbf{H}}{dt}$ were again observed, which we labeled D, E, and F (Figure 5, Table 4). On October 10, at approximately 15:00 UT, the arrival of a CME was observed by a sudden commencement, Spike D. All of mainland New Zealand experienced a roughly equivalent magnetic field spike (an expected response to a SSC), with a slightly weaker variation in the Chathams to the east. As the storm continued, it intensified at southern sites, until it peaked again at 23:10 UT on 10 October, spike E. Spike E shows a smooth increase in the magnitude of $\frac{d\mathbf{H}}{dt}$ from north to south, peaking at 132 nT/min in Awarua. Spike E appears to be related to a global feature at the end of a ring current enhancement noted by Kleimenova et al. (2025). A dramatic drop in solar wind pressure and a sudden flip in IMF Bz from positive to negative occurred. Later during the storm, at approximately 10:15 UT on 11 October a third spike, spike F, was observed. However, in this case, no significant magnetic variation was observed at Donnelly or Chathams. A small spike of 40 nT/min was measured at Eyrewell, while a large spike was present at Swampy and Awarua, 182 nT/min and 202 nT/min, respectively. This was likely due to a substorm expansion (see Section 4.3).

Overall, October 2024 was much weaker than the Gannon storm, though still a significant event. In terms of $\frac{d\mathbf{H}}{dt}$ at Eyrewell, the peak at spike E of 117 nT/min marks this storm as the fifth largest since 1994 (Rodger et al., 2017). The variability across New Zealand for Spike F also demonstrates how Eyrewell was unable to capture the full extent of magnetic variability across New Zealand, with significant activity observed in the very south of New Zealand.

4.3. SME Index

For the May 2024 storm, spikes B and C coincide with substorm activity, as shown in Figure 6. Spike B and C occur during large SML spikes when New Zealand was on the night side of the Earth (20:55 and 00:30 MLT). We suspect that both of these substorm enhancements led to spikes B and C in the magnetic field variation. Spike B was noticeably stronger further north, particularly at Eyrewell. This may be due to the large amplitude of the substorm (SML $< -2{,}500$ nT), a point that we address later in the discussion (Section 5.1).

For 11 October, no SML peak was observed during Spike F (with SML in recovery from a previous peak at roughly 08:50), unexpectedly (nor is it listed in the SOPHIE substorm list, https://supermag.jhuapl.edu/substorms/). No abrupt changes in solar wind conditions were observed during this time (Oliveira et al., 2025). Spike F is localized in $\frac{d\mathbf{H}}{dt}$ to the southernmost sites and is located on the night side (22:40 MLT), which is typical for a substorm. Magnetic time series taken from INTERMAGNET at roughly the equivalent magnetic latitude and longitude at Shumagin, Alaska also displayed this peak at spike F (see Figure A1 in Appendix A).

Two possibilities could explain this peak:

1. The SME index missed the substorm, due to a lack of magnetometers within the range (i.e., ±30°) of the geomagnetic meridian of New Zealand used in its calculation.

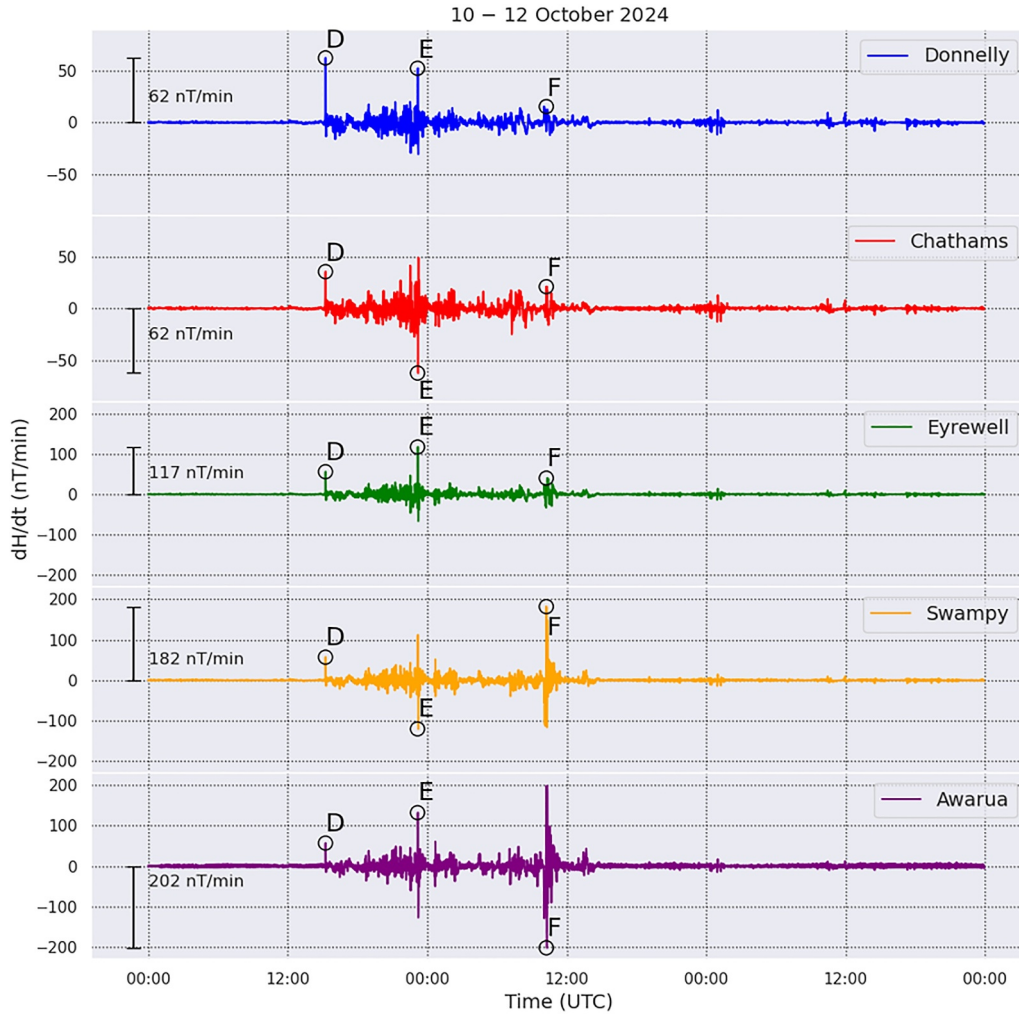

Figure 5. The rate of change of the magnetic field (**H**) for the October 2024 storm, arranged from northernmost to southernmost (i.e., equatorward to poleward). Three main spikes of note denoted by D, E, and F occurred at approximately 15:15 UT, 23:10 UT, 10 October 2024, and 10:15 UT, 11 October 2024. The largest magnetic field variations were observed for the southernmost observatories, peaking at 202 nT/min at Awarua and 182 nT/min at Swampy for the spike F. The Oakview site suffered an outage for this storm and hence was not plotted.

2. A localized extreme during the storm occurred in a narrow latitudinal/longitudinal band related to the night side magnetotail. An example of this could be dipolarizing flux bundles (Engebretson et al., 2019, 2024).

These possibilities were considered in more detail in the discussion (Section 5.2.2).

Table 4
*The Absolute Value of Peaks Observed for the Rate of Change of the Horizontal Magnetic Field, **H**, in Figure 5 During the October 2024 Storm at Each Site*

Site	Spike D 15:15 UT (nT/min)	Spike E 23:10 UT (nT/min)	Spike F 10:15 UT (nT/min)
Donnelly	62	52	15
Chathams	36	62	21
Eyrewell	56	117	40
Swampy	57	120	182
Awarua	57	132	202

4.4. H30-Index and Hpo-Index

The H30-index and Hp30-index are plotted to compare the global activity to magnetometer activity at Eyrewell and Awarua during the May and October 2024 storms (Figures 8 and 9). For both the Gannon and October storms, the Hp30-index generally exceeds the local H30-index, although the local H30-index was larger at its peak value.

For the Gannon storm, the local H30-index at Eyrewell and Awarua (upper two panels of Figure 8) was weaker than the global Hp30-index (lower panel of Figure 8) for spike A ($H30_{eyr} = 9$, $H30_{awa} = 9$ and $Hp30 = 11+$). As mentioned in Section 4.1, a ring current enhancement was the likely source of this peak. Locally, the effect of this enhancement must have been small. Spike

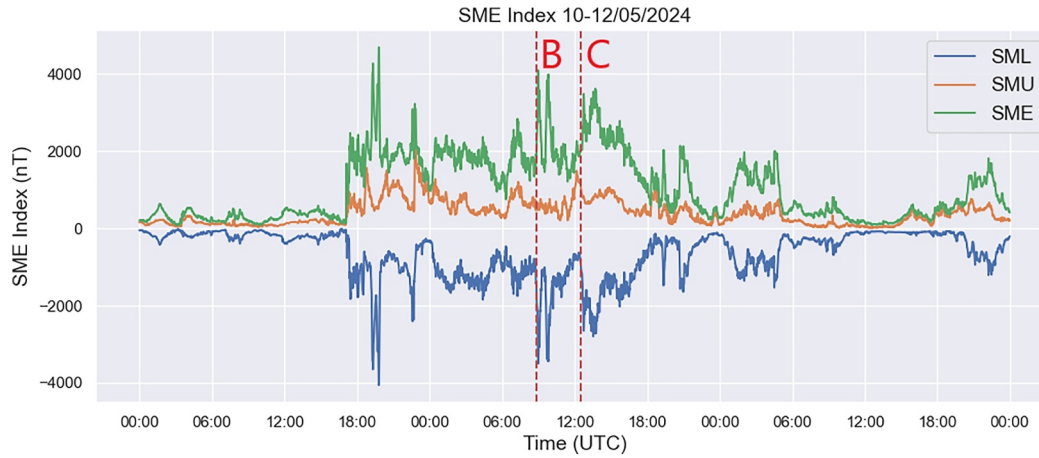

Figure 6. The SuperMAG auroral electrojet index (SME) during the 10–12 May 2024 geomagnetic storm. The red dashed line is used to denote the timings of possible substorms for NZ. The westward (SML) and eastward (SMU) indices are also shown. Two substorm expansions are visible at the times of the largest rate of change in the geomagnetic field in Figure 4.

B was much greater at Eyrewell and Awarua than globally ($H30_{eyr} = 14$, $H30_{awa} = 13$ and $Hp30 = 9o$). We hypothesize that spike B was due to a substorm expansion (Figure 8, 20:50 MLT), hence global activity would be much weaker. Spike C was slightly greater at Eyrewell than in the global Hp30, and much greater at Awarua ($H30_{eyr} = 11$, $H30_{awa} = 12$, $Hp30 = 9o$). A substorm expansion was again the likely cause of this (Figure 6, 00:30 MLT). It appears that in this case, Eyrewell was only weakly impacted by the substorm compared to spike B, a point which we later address in the discussion (Section 5.1).

For the October storm, shown in Figure 7, spike D (i.e., the SSC) was roughly equivalent at Eyrewell, Awarua and globally ($H30_{eyr} = 7$, $H30_{awa} = 6$, $Hp30 = 7o$). Spike E, related to a ring current enhancement and a rapid change in solar wind conditions (Kleimenova et al., 2025), was significantly weaker at Eyrewell and Awarua than globally ($H30_{eyr} = 8$, $H30_{awa} = 8$, $Hp30 = 10+$). Spike F was comparable at Eyrewell and much stronger at Awarua, compared to global activity ($H30_{eyr} = 8$, $H30_{awa} = 13$, $Hp30 = 7+$). This adds more evidence to support the hypothesis that a substorm was responsible for this peak at Awarua (22:40 MLT).

Comparing the H30-indices for the May and October storms, we see that both storms were exceptional events, exceeding the severe storm threshold of $H30 = 9$. It can quickly be observed that the May storm was much larger than the October storm at Eyrewell ($H30_{eyr} = 14$ vs. 9) and though similar at Awarua ($H30_{awa} = 13$ vs. 13).

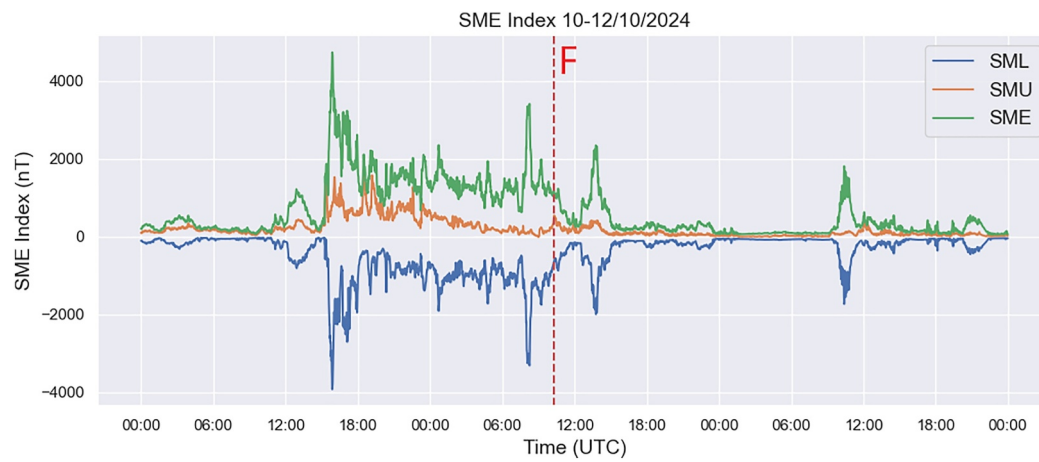

Figure 7. The SuperMAG auroral electrojet index during the 10–12 October 2024 geomagnetic storm. The westward (SML) and eastward (SMU) indices are also shown. The red dashed line is used to denote timings of possible substorms for NZ. No apparent activity was observed in the SME index at 10:15 UT, when the largest localized spike in $\frac{d\mathbf{H}}{dt}$ plotted in Figure 5 occurs.

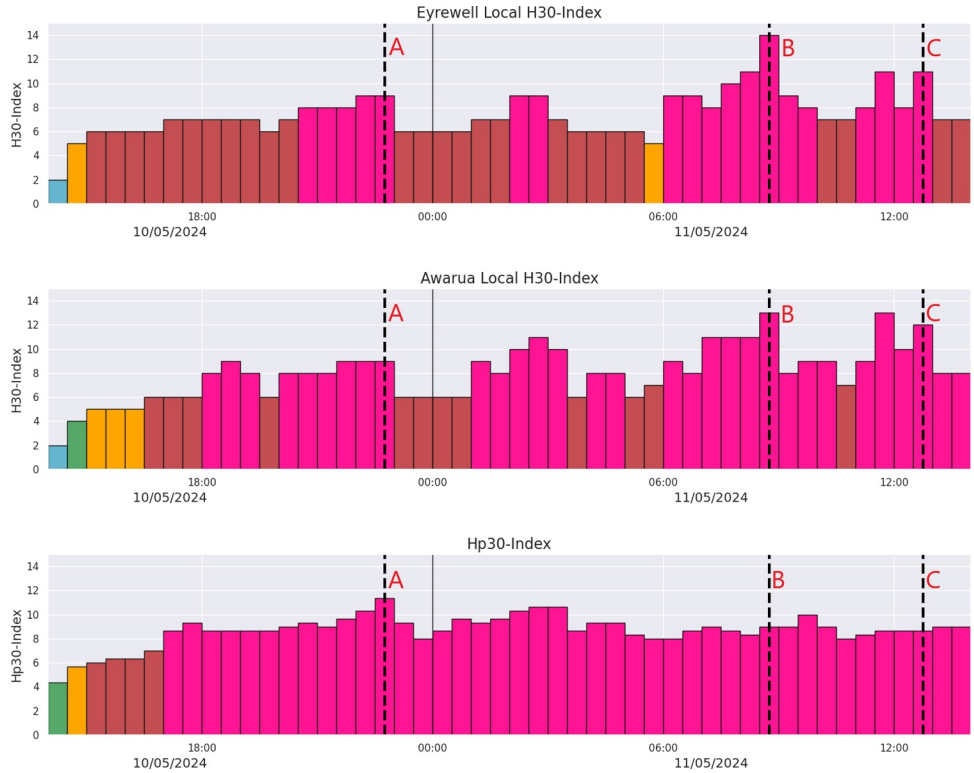

Figure 8. H30- and Hp30-indices for the Eyrewell and Awarua sites on the 10–11/05/2024 during the peak of the May storm. The three major spikes from Figure 4 are denoted by A, B and C.

5. Discussion

5.1. Evaluation of the May and October 2024 Storms

The Gannon storm was the largest geomagnetic storm in terms of $\frac{d\mathbf{H}}{dt}$ at Eyrewell since the beginning of digital records, peaking at 320 nT/min. Local enhancements from substorms enhanced the magnetic field variations at Eyrewell up to this peak level. While the Gannon storm was a globally severe event, the H30- and Hp30-indices demonstrate that this storm was particularly severe for New Zealand.

The most likely explanation for this discrepancy between global and local activity is related to substorm expansions. Spikes B and C were most likely related to substorms based on SME/L/U (Figure 6) and localized activity in H30 (Figure 8). Spike B was quite an unusual spike, as a large peak in the magnetic field for the substorm expansion was observed as far equatorward as Eyrewell. A substantial spike even occurred as far north as the Chathams. The reported SML index at that time (SML ≈ -3500 nT) meets the criteria for a so-called supersubstorm, an extremely intense substorm, SML $< -2{,}500$ nT (Tsurutani et al., 2015). At the same instant as spike B, a distinct solar wind pressure pulse was observed by Zou et al. (2025), a feature often observed during these extreme substorms and hypothesized to trigger some of these events (Tsurutani et al., 2015). This pressure pulse may help explain why the substorm expansion was so strong, extending the auroral oval much further equatorward. In comparison, spike C also falls in the supersubstorm range (SML $\approx -2{,}750$ nT). However, no clear solar wind pressure pulse was observed or reported (e.g., Hajra et al., 2024). More likely a more conventional substorm drove this event, that is, unrelated to a solar wind pressure pulse. The magnetic variation is significantly weaker at Eyrewell during spike C than during spike B (130 nT/min); however, it was much larger in the south of New Zealand at Swampy and Awarua (360 and 478 nT/min respectively). The substorm at spike C is still observed at latitudes unusually far north, though not to the same extent as found during spike B, with the magnitude difference observed by SME potentially indicating the cause of the auroral oval not expanding as far equatorward.

10.1029/2025SW004629

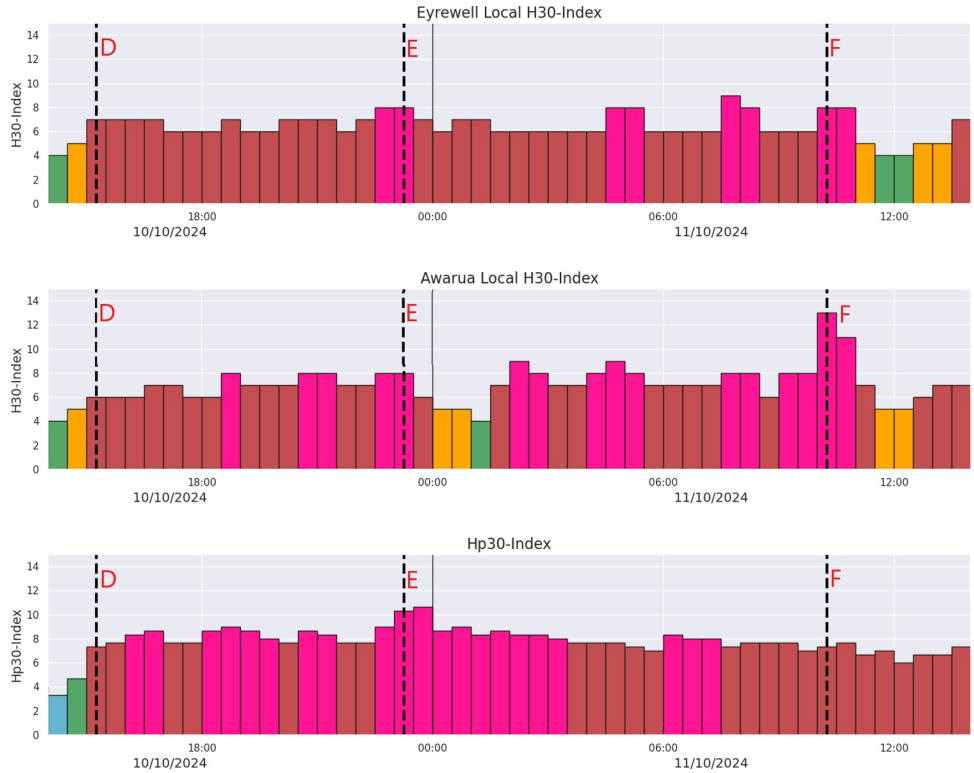

Figure 9. H30- and Hp30-indices for the Eyrewell and Awarua sites on the 10–11/10/2024 during the peak of the October storm. The three major spikes from Figure 5 are denoted by D, E and F.

In contrast to the Gannon storm, the H30- and Hp30-indices demonstrate that New Zealand was probably not impacted as much for the October 2024 storm as the rest of the world (with the exception of spike F at Awarua and Swampy). Spikes D and E were notable, but weak compared to the spikes of May 2024. Spike D was related to the initial SSC, while spike E is related to an enhancement of the ring current. Spike F is a more interesting case. A clear localized disturbance occurs in the very south at Awarua and Swampy. The spike resembles a substorm, though the SME index suggests otherwise. We hypothesize that spike F is indeed related to a substorm, and that a spatial bias in the location of the magnetometers used to determine SME is to blame, as comparable spikes were observed at other magnetometers at similar latitudes in the Northern Hemisphere (see Figure A1 in Appendix A). This point is discussed further in Section 5.2.2. Although relatively weaker, spike F still produced a peak of 202 nT/min at Awarua and at Eyrewell was the fifth largest geomagnetic storm since 1994 in terms of $\frac{d\mathbf{H}}{dt}$ for spike E.

To help explain exactly how extreme the Gannon storm was, a quick comparison with historical events can yield some insight. The famous Hydro-Quebec failure of 1989 corresponded to a max $\frac{d\mathbf{H}}{dt}$ of 479 nT/min (Fiori et al., 2014). An equivalent magnetic field variation was observed at Awarua for the Gannon storm (478 nT/min). Although the Gannon storm was the largest storm since 1994 in NZ, historically much more extreme storms have been measured by magnetometers in New Zealand, most notably the May 1921 storm (Skey, 1921). Although there was no substantial power infrastructure in 1921, telegraph lines were severely disrupted during the geomagnetic storm, and it was estimated that the center of the auroral electrojet was directly over Auckland, in the north of New Zealand, based on auroral observations (Silverman & Cliver, 2001). This expansion is approximately 10° further equatorward than that observed for the Gannon storm. With regard to a roughly 1-in-500-year storm, an extreme event even greater than the May 1921 event, a $\frac{d\mathbf{H}}{dt} \approx$ 4,000 nT/min and 5,500 nT/min are estimated at latitudes equivalent to Eyrewell and Awarua, respectively, by Mac Manus et al. (2022), based on estimates by the statistical model of Rogers et al. (2020). A maximum GIC estimate of approximately 2,000–5,000 A for such a scenario in New Zealand was estimated (Mac Manus et al., 2022). So, while the Gannon storm was large, much larger storms can occur over longer timescales, which are likely to negatively impact power networks and other vulnerable infrastructure.

5.2. Benefits of the MANA Network

5.2.1. MANA and the Impact on GIC Modeling in New Zealand

The addition of the MANA magnetometer array to the existing Eyrewell geomagnetic observatory has demonstrated that the very south of NZ is impacted by much larger magnetic field variations than previously thought. In turn, this has led to a larger predicted GIC in the power grid. For the May 2024 event, Mac Manus et al. (2025) reported that the largest GIC ever measured in the New Zealand power grid of 113 A and expected a GIC in excess of 200 A, had Transpower New Zealand not enacted a mitigation plan designed to lower the GIC during the storm (Mac Manus, 2023; Mac Manus et al., 2023). Mac Manus et al. (2025) reported that this GIC peak occurred during spike C. Although the magnetic field variation was relatively weak at Eyrewell, a much larger variation was observed at Swampy and Awarua which generated this very large GIC. Previously, it was thought in NZ that sudden impulses and sudden storm onsets were more likely to be responsible for the largest magnetic field variations and hence, large GIC in NZ, given that it is a mid-latitude country (Rodger et al., 2017; Smith et al., 2024). This is likely to remain true for most of NZ. However, the addition of the new magnetometer network demonstrated that substorm expansions can generate serious magnetic field variations in the very South of NZ, even larger than those previously observed during SSC. It should also be noted that the second largest recorded GIC also occurred during a substorm during the September 2017 storm (Mac Manus et al., 2022; Rodger et al., 2020). Mac Manus et al. (2025) also reports a large improvement in the modeling of GIC during the May 2024 storm, when modeling using the entire MANA network. Overall, the MANA network has helped reveal this vulnerability to substorms. A future goal of the Solar Tsunamis project will be to quantify the improvement due to the addition of the MANA network.

In addition to modeling GIC in power grids, the network has also been useful in terms of determining GIC in pipelines. Ingham et al. (2022); Divett et al. (2023) originally developed a model of GIC in pipelines based on magnetometer measurements from Eyrewell alone. Most of this infrastructure is located around the center of the North Island, >400 km away from the Eyrewell observatory. Divett et al. (2024) demonstrated for the Gannon storm, that using magnetic field inputs from Oakview improved GIC modeling across the North Island. The network can also be used for geological aspects, such as the mapping of lithospheric conductivity profiles from magnetotelluric surveys (Pratscher et al., 2024), which benefits GIC modeling in power lines and pipelines (Cordell et al., 2021, 2024; Ingham et al., 2023; Kelbert & Lucas, 2020; Marshalko et al., 2023).

5.2.2. MANA for Monitoring Geomagnetic Storms

An objective of the MANA network is to monitor geomagnetic storms across New Zealand in real time. To effectively monitor the potential impact from GIC during geomagnetic storms with magnetometer data, both rapid- and slower-scale activity must be accounted for. Very rapid changes in the magnetic field can cause a series of power grid malfunctions, such as circuit breaker tripping and reduced performance of voltage control systems, which can ultimately lead to a failure, such as the Quebec blackout in 1989 (Bolduc, 2002). Similarly, railway signaling failures are also more susceptible to these large rapid variations (Patterson et al., 2024; Wik et al., 2009). $\frac{d\mathbf{H}}{dt}$ is very useful to identify this type of activity. The main issue with using $\frac{d\mathbf{H}}{dt}$ alone to quantify magnetic activity is that it lacks the memory to identify slower-scale, directionally polarized activity (Kellinsalmi et al., 2022). Sustained magnetic variations can lead to sustained GIC, which can cause saturation and overheating in transformers in power grids and, in extreme cases, damage transformers beyond repair (Gaunt & Coetzee, 2007). In pipelines, sustained activity is also the main culprit of corrosion and damage (Pulkkinen et al., 2001).

We demonstrated an example here of how both $\frac{d\mathbf{H}}{dt}$ and H30-indices can be used to evaluate both rapid and sustained magnetic activity. The best example of this is spike D, related to the SSC in October 2024. $\frac{d\mathbf{H}}{dt}$ observes a distinct peak across the islands (≈60 nT/min), although H30 only marks spike D as a moderate storm (H30 = 6, Hp30 = 6). $\frac{d\mathbf{H}}{dt}$ is especially useful for identifying these sudden sharp changes in the magnetic field. In contrast to $\frac{d\mathbf{H}}{dt}$, Hpo is better at identifying and quantifying slower-varying magnetic fields. The best example of this was later during the October 2024 storm. Between spike E and F, at 08:45 UT, the largest value of $H30_{eyr}$ = 9 was observed at Eyrewell. Sustained activity was present in $\frac{d\mathbf{H}}{dt}$ at Eyrewell, however no spike >25 nT/min was observed. Given that GIC can be harmful both due to sharp sudden changes, as well as sustained directionally polarized activity, each of these are valuable tools (Béland & Small, 2005; Heyns et al., 2021). Currently $\frac{d\mathbf{H}}{dt}$ is

monitored on the MANA website and in the future we plan to add H30-indices as well. This is because understandably, local indices can more accurately derive local geomagnetic conditions (e.g., Cid et al., 2020) while simultaneously, these indices can also be easily compared to global activity, an added benefit.

Spikes B, C and F showed the importance of considering localized variations within the network. The unusual spike F at Awarua and Swampy is the best example of this. While it appeared to be a substorm (Figure 5), the SME index suggests otherwise (Figure 7). As stated in the observations, we believe that this was due to an asymmetry in the SME index itself. Rather than a lack of magnetometers in the Northern hemisphere, which can cause biases not observed in the Southern Hemisphere (Weygand et al., 2014), in this case it was most likely due to the lack of magnetometers in the Pacific region. In general, magnetometers in the Pacific are rare, and the addition of the new MANA network provides a new observation point globally. However, this assumption that the spike is a substorm is still debatable; a global study would be better at deciphering this. A geomagnetic disturbance caused by dipolarizing flux bundles (DFB) was offered as an alternate hypothesis. DFBs are small transient magnetotail flux tubes located in the magnetotail of the Earth, which can disturb ground-based magnetometers in the pre-midnight sector, with a latitudinal/longitudinal range of approximately 250–450 km (i.e., highly localized compared to a typical substorm), by amplifying the westward auroral electrojet (Engebretson et al., 2024; Weygand et al., 2021). However, observing such a disturbance so far equatorward would be a first (Mlat 50–54°). Hence, we assume the former. With the current density of magnetometers in the region, this would be difficult to confirm either way. Nevertheless, spikes B, C and F prove that the southernmost magnetometers of Awarua and Swampy are particularly important for accurately replicating geomagnetic storms across New Zealand. Due to the scarcity of magnetic field observations from this region of the world, MANA is also useful in a global sense.

6. Conclusions

1. The new MANA magnetometer network was presented. This included specifications of the equipment used and technical details regarding the installation. The capabilities of the network were also explored. The network will improve GIC modeling across the Islands (and has already begun to do so), as well as assist other studies reliant on magnetic field measurements such as other space weather phenomena (e.g., radiation belts) and magnetotellurics.
2. Observations from the Gannon and October 2024 storms were reported from across New Zealand. Eyrewell experienced the largest $\frac{d\mathbf{H}}{dt}$ since 1994 during the Gannon storm, while large magnetic fields were observed across NZ during the October storm. During both storms at the southernmost Awarua and Swampy sites (and to a lesser extent Eyrewell), substorm expansions appeared to cause the largest magnetic variations, while variations related to the ring current and SSC were more dominant further north. No damage was reported to the NZ power grid due to the Gannon storm, although the effects of the storm on the power grid were mitigated (Mac Manus et al., 2025).

Appendix A

Figure A1

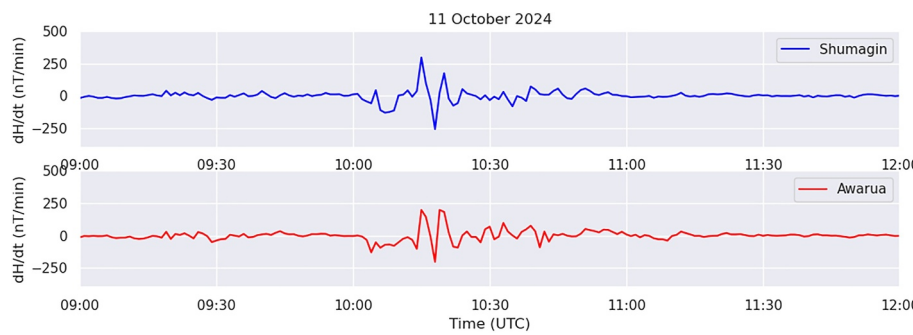

Figure A1. The rate of change of the **H** component of the magnetic field from 11 October 2024, during Spike F. The same spike observed at Awarua (−54.04°, 254.68°, CGM) was also observed at Shumagin, Alaska, USA (53.20°, 259.27°, CGM) at roughly the same latitude and longitude in opposite hemispheres.

Conflict of Interest

The authors declare no conflicts of interest relevant to this study.

Data Availability Statement

The computational Python scripts used to derive the H30-indices and $\frac{d\mathbf{H}}{dt}$ were created by Malone-Leigh (2025), where the sample time series can also be found. The scripts used to generate H30-indices were adapted from scripts developed to calculate K-indices, developed by the Trinity College Dublin/Dublin Institute for Advanced Studies Solar Physics Group (Blake, 2017; Malone-Leigh, 2024). We gratefully acknowledge the use of the Hpo-indices, provided by GFZ Potsdam (Matzka et al., 2024). The IGRF CGM coordinates at magnetometer sites were calculated via the OMNI database (https://omniweb.gsfc.nasa.gov/vitmo/cgm.html). Magnetic local times were calculated using apexpy (Emmert et al., 2010). We acknowledge use of NASA/GSFC's Space Physics Data Facility's OMNIWeb (or CDAWeb or ftp) service, and OMNI data. SuperMAG indices SME, SMU and SML were obtained from https://supermag.jhuapl.edu/indices/. We gratefully acknowledge the SuperMAG collaborators (https://supermag.jhuapl.edu/info/?page=acknowledgement). The results presented in this paper rely on the data collected at the Eyrewell and Shumagin geomagnetic observatories. We thank Earth Sciences New Zealand and the US Geological Survey for supporting their operation and INTERMAGNET for promoting high standards of magnetic observatory practice (www.intermagnet.org).

Acknowledgments
We would like to thank the New Zealand Ministry for Business Innovations and Employment for funding the MANA network as part of Solar Tsunamis. We thank Earth Sciences New Zealand (formerly GNS Science) for hosting, maintaining, and providing real-time data. We thank Space Operations New Zealand for hosting the Awarua magnetometer site. This study was supported by the New Zealand Ministry of Business, Innovation, & Employment through Endeavour Fund Research Programme contract UOOX2002.

References

Abe, O., Fakomiti, M., Igboama, W., Akinola, O., Ogunmodimu, O., & Migoya-Orué, Y. (2023). Statistical analysis of the occurrence rate of geomagnetic storms during solar cycles 20–24. *Advances in Space Research*, *71*(5), 2240–2251. https://doi.org/10.1016/j.asr.2022.10.033

Alken, P., Thébault, E., Beggan, C. D., Amit, H., Aubert, J., Baerenzung, J., et al. (2021). International geomagnetic reference field: The thirteenth generation. *Earth Planets and Space*, *73*(1), 49. https://doi.org/10.1186/s40623-020-01288-x

Bartels, J., Heck, N. H., & Johnston, H. F. (1939). The three-hour-range index measuring geomagnetic activity. *Terrestrial Magnetism and Atmospheric Electricity*, *44*(4), 411–454. https://doi.org/10.1029/TE044i004p00411

Belakhovsky, V., Pilipenko, V., Engebretson, M., Sakharov, Y., & Selivanov, V. (2019). Impulsive disturbances of the geomagnetic field as a cause of induced currents of electric power lines. *Journal of Space Weather and Space Climate*, *9*, A18. https://doi.org/10.1051/swsc/2019015

Béland, J., & Small, K. (2005). Space weather effects on power transmission systems: The cases of Hydro-Québec and Transpower New Zealand Ltd. In I. A. Daglis (Ed.), *Effects of space weather on technology infrastructure* (pp. 287–299). Springer Netherlands. https://doi.org/10.1007/1-4020-2754-0_15

Bergin, A., Chapman, S. C., & Gjerloev, J. W. (2020). AE, D, and their supermag counterparts: The effect of improved spatial resolution in geomagnetic indices. *Journal of Geophysical Research: Space Physics*, *125*(5), e2020JA027828. https://doi.org/10.1029/2020JA027828

Blake, S. P. (2017). *Modelling and monitoring geomagnetically induced currents in Ireland*. Doctoral dissertation. Trinity College Dublin. Retrieved from https://hdl.handle.net/2262/1101749

Bolduc, L. (2002). GIC observations and studies in the Hydro-Québec power system. *Journal of Atmospheric and Solar-Terrestrial Physics*, *64*(16), 1793–1802. https://doi.org/10.1016/s1364-6826(02)00128-1

Boteler, D. (2006). The super storms of August/September 1859 and their effects on the telegraph system. *Advances in Space Research*, *38*(2), 159–172. (The Great Historical Geomagnetic Storm of 1859: A Modern Look). https://doi.org/10.1016/j.asr.2006.01.013

Campanyà, J., Gallagher, P. T., Blake, S. P., Gibbs, M., Jackson, D., Beggan, C., et al. (2019). Modeling geoelectric fields in Ireland and the UK for space weather applications. *Space Weather*, *17*(2), 216–237. https://doi.org/10.1029/2018SW001999

Cid, C., Guerrero, A., Saiz, E., Halford, A. J., & Kellerman, A. C. (2020). Developing the LDi and LCi geomagnetic indices, an example of application of the AULs framework. *Space Weather*, *18*(1), e2019SW002171. https://doi.org/10.1029/2019SW002171

Clilverd, M. A., Rodger, C. J., Brundell, J. B., Dalzell, M., Martin, I., Mac Manus, D. H., & Thomson, N. R. (2020). Geomagnetically induced currents and harmonic distortion: High time resolution case studies. *Space Weather*, *18*(10), e2020SW002594. https://doi.org/10.1029/2020SW002594

Clilverd, M. A., Rodger, C. J., Manus, D. H. M., Brundell, J. B., Dalzell, M., Renton, A., et al. (2025). Geomagnetically induced currents, transformer harmonics, and reactive power impacts of the Gannon storm in May 2024. *Space Weather*, *23*(4), e2024SW004235. https://doi.org/10.1029/2024SW004235

Cordell, D., Mann, I. R., Dimitrakoudis, S., Parry, H., & Unsworth, M. J. (2025). Long-term peak geoelectric field behavior for space weather hazard assessment in Alberta, Canada using geomagnetic and magnetotelluric measurements. *Space Weather*, *23*(3), e2024SW004305. https://doi.org/10.1029/2024SW004305

Cordell, D., Mann, I. R., Parry, H., Unsworth, M. J., Cui, R., Clark, C., et al. (2024). Modeling geomagnetically induced currents in the Alberta power network: Comparison and validation using hall probe measurements during a magnetic storm. *Space Weather*, *22*(4), e2023SW003813. https://doi.org/10.1029/2023SW003813

Cordell, D., Unsworth, M. J., Lee, B., Hanneson, C., Milling, D. K., & Mann, I. R. (2021). Estimating the geoelectric field and electric power transmission line voltage during a geomagnetic storm in Alberta, Canada using measured magnetotelluric impedance data: The influence of three-dimensional electrical structures in the lithosphere. *Space Weather*, *19*(10), e2021SW002803. https://doi.org/10.1029/2021SW002803

De Michelis, P., & Consolini, G. (2025). Unveiling the Gannon storm: How ground-based magnetometers mapped its global impact. *Space Weather*, *23*(6), e2025SW004350. https://doi.org/10.1029/2025SW004350

Dimmock, A., Rosenqvist, L., Welling, D., Viljanen, A., Honkonen, I., Boynton, R., & Yordanova, E. (2020). On the regional variability of d b/dt and its significance to GIC. *Space Weather*, *18*(8), e2020SW002497. https://doi.org/10.1029/2020SW002497

Divett, T., Ingham, M., Richardson, G., Sigley, M., & Rodger, C. J. (2023). Modeling pipe to soil potentials from geomagnetic storms in gas pipelines in New Zealand. *Space Weather*, *21*(12), e2023SW003601. https://doi.org/10.1029/2023SW003601

Divett, T., Ingham, M., Sigley, M., Pratscher, K., Petersen, T., Heise, W., & Rodger, C. (2024). Validating modelled pipe to soil potentials and GICS in New Zealand's gas pipelines. *European Space Weather Week*.

Elvidge, S., & Themens, D. R. (2025). The probability of the May 2024 geomagnetic superstorm. *Space Weather*, *23*(1), e2024SW004113. https://doi.org/10.1029/2024SW004113

Emmert, J. T., Richmond, A. D., & Drob, D. P. (2010). A computationally compact representation of Magnetic-Apex and Quasi-Dipole coordinates with smooth base vectors. *Journal of Geophysical Research*, *115*(A8), A08322. https://doi.org/10.1029/2010JA015326

Engebretson, M. J., Gaffaney, S. A., Ochoa, J. A., Runov, A., Weygand, J. M., Nishimura, Y., et al. (2024). Signatures of dipolarizing flux bundles in the nightside auroral zone. *Journal of Geophysical Research: Space Physics*, *129*(4), e2023JA032266. https://doi.org/10.1029/2023JA032266

Engebretson, M. J., Pilipenko, V. A., Ahmed, L. Y., Posch, J. L., Steinmetz, E. S., Moldwin, M. B., et al. (2019). Nighttime magnetic perturbation events observed in arctic Canada: 1. Survey and statistical analysis. *Journal of Geophysical Research: Space Physics*, *124*(9), 7442–7458. https://doi.org/10.1029/2019JA026794

Fiori, R. A. D., Boteler, D. H., & Gillies, D. M. (2014). Assessment of GIC risk due to geomagnetic sudden commencements and identification of the current systems responsible. *Space Weather*, *12*(1), 76–91. https://doi.org/10.1002/2013SW000967

Fogg, A. R., Jackman, C. M., Malone-Leigh, J., Gallagher, P. T., Smith, A. W., Lester, M., et al. (2023). Extreme value analysis of ground magnetometer observations at Valentia observatory, Ireland. *Space Weather*, *21*(7), e2023SW003565. https://doi.org/10.1029/2023SW003565

Gaunt, C. T., & Coetzee, G. (2007). Transformer failures in regions incorrectly considered to have low GIC-risk. In *2007 IEEE Lausanne power tech* (pp. 807–812). https://doi.org/10.1109/PCT.2007.4538419

Gjerloev, J. W. (2012). The supermag data processing technique. *Journal of Geophysical Research*, *117*(A9). https://doi.org/10.1029/2012JA017683

Hajra, R., Tsurutani, B. T., Lakhina, G. S., Lu, Q., & Du, A. (2024). Interplanetary causes and impacts of the 2024 May superstorm on the geosphere: An overview. *The Astrophysical Journal*, *974*(2), 264. https://doi.org/10.3847/1538-4357/ad7462

Hartinger, M. D., Shi, X., Rodger, C. J., Fujii, I., Rigler, E. J., Kappler, K., et al. (2023). Determining ULF wave contributions to geomagnetically induced currents: The important role of sampling rate. *Space Weather*, *21*(5), e2022SW003340. https://doi.org/10.1029/2022SW003340

Hayakawa, H., Ebihara, Y., Mishev, A., Koldobskiy, S., Kusano, K., Bechet, S., et al. (2025). The solar and geomagnetic storms in 2024 May: A flash data report. *The Astrophysical Journal*, *979*(1), 49. https://doi.org/10.3847/1538-4357/ad9335

Hendry, A. T., Rodger, C. J., Clilverd, M. A., Engebretson, M. J., Mann, I. R., Lessard, M. R., et al. (2016). Confirmation of emic wave-driven relativistic electron precipitation. *Journal of Geophysical Research: Space Physics*, *121*(6), 5366–5383. https://doi.org/10.1002/2015JA022224

Heyns, M. J., Lotz, S. I., & Gaunt, C. T. (2021). Geomagnetic pulsations driving geomagnetically induced currents. *Space Weather*, *19*(2), e2020SW002557. https://doi.org/10.1029/2020SW002557

Hübert, J., Beggan, C. D., Richardson, G. S., Martyn, T., & Thomson, A. W. P. (2020). Differential magnetometer measurements of geomagnetically induced currents in a complex high voltage network. *Space Weather*, *18*(4), e2019SW002421. https://doi.org/10.1029/2019SW002421

Ingham, M., Divett, T., Rodger, C. J., & Sigley, M. (2022). Impacts of GIC on the New Zealand gas pipeline network. *Space Weather*, *20*(12), e2022SW003298. https://doi.org/10.1029/2022SW003298

Ingham, M., Divett, T., Rodger, C. J., & Sigley, M. (2025). Observed effects of the May 2024 Gannon storm on the New Zealand gas pipeline network—Toward predicting the effects of an extreme storm. *Space Weather*, *23*(5), e2024SW004258. https://doi.org/10.1029/2024SW004258

Ingham, M., Pratscher, K., Heise, W., Bertrand, E., Kruglyakov, M., & Rodger, C. J. (2023). Influence of tectonic and geological structure on GIC in southern south island, New Zealand. *Space Weather*, *21*(11), e2023SW003550. https://doi.org/10.1029/2023SW003550

Juusola, L., Kauristie, K., Vanhamäki, H., Aikio, A., & van de Kamp, M. (2016). Comparison of auroral ionospheric and field-aligned currents derived from swarm and ground magnetic field measurements. *Journal of Geophysical Research: Space Physics*, *121*(9), 9256–9283. https://doi.org/10.1002/2016JA022961

Kelbert, A., & Lucas, G. M. (2020). Modified GIC estimation using 3-D Earth conductivity. *Space Weather*, *18*(8), e2020SW002467. https://doi.org/10.1029/2020SW002467

Kellinsalmi, M., Viljanen, A., Juusola, L., & Käki, S. (2022). The time derivative of the geomagnetic field has a short memory. *Annales Geophysicae*, *40*(4), 545–562. https://doi.org/10.5194/angeo-40-545-2022

Kleimenova, N., Gromova, L., Gromov, S., & Malysheva, L. (2025). Planetary feature of the ionospheric current activity during 10–11 October 2024 extremely strong magnetic storm. *Journal of Atmospheric and Solar-Terrestrial Physics*, *277*, 106631. https://doi.org/10.1016/j.jastp.2025.106631

Lawrence, E., Beggan, C. D., Richardson, G. S., Reay, S., Thompson, V., Clarke, E., et al. (2025). The geomagnetic and geoelectric response to the May 2024 geomagnetic storm in the United Kingdom. *Frontiers in Astronomy and Space Sciences*, *12*, 1550923. https://doi.org/10.3389/fspas.2025.1550923

Love, J. J., & Chulliat, A. (2013). An international network of magnetic observatories. *Eos, Transactions American Geophysical Union*, *94*(42), 373–374. https://doi.org/10.1002/2013EO420001

Lugaz, N., Knipp, D., Morley, S. K., Liu, H., Hapgood, M., Carter, B., et al. (2024). In memoriam of editor Jennifer L. Gannon. *Space Weather*, *22*(6), e2024SW004016. https://doi.org/10.1029/2024SW004016

Mac Manus, D. H. (2023). *Geomagnetically induced currents: Validating observations and modelling in New Zealand.* Doctoral dissertation. School of Physics. Retrieved from https://hdl.handle.net/10523/15443

Mac Manus, D. H., Rodger, C. J., Dalzell, M., Thomson, A. W. P., Clilverd, M. A., Petersen, T., et al. (2017). Long-term geomagnetically induced current observations in New Zealand: Earth return corrections and geomagnetic field driver. *Space Weather*, *15*(8), 1020–1038. https://doi.org/10.1002/2017SW001635

Mac Manus, D. H., Rodger, C. J., Ingham, M., Clilverd, M. A., Dalzell, M., Divett, T., et al. (2022). Geomagnetically induced current model in New Zealand across multiple disturbances: Validation and extension to non-monitored transformers. *Space Weather*, *20*(2), e2021SW002955. https://doi.org/10.1029/2021SW002955

Mac Manus, D. H., Rodger, C. J., Renton, A., Lo, V., Malone-Leigh, J., Petersen, T., et al. (2025). Implementing geomagnetically induced currents mitigation during the May 2024 "Gannon" G5 storm: Research informed response by the New Zealand power network. *Space Weather*, *23*(6), e2025SW004388. https://doi.org/10.1029/2025SW004388

Mac Manus, D. H., Rodger, C. J., Renton, A., Ronald, J., Harper, D., Taylor, C., et al. (2023). Geomagnetically induced current mitigation in New Zealand: Operational mitigation method development with industry input. *Space Weather*, *21*(11), e2023SW003533. https://doi.org/10.1029/2023SW003533

Malone-Leigh, J. (2024). Monitoring and modelling geomagnetic and geoelectric fields in Ireland. Doctoral dissertation. Retrieved from http://hdl.handle.net/2262/108568

Malone-Leigh, J. (2025). *H30 indices*. Zenodo. https://doi.org/10.5281/zenodo.15946231

Malone-Leigh, J., Campanyà, J., Gallagher, P. T., Neukirch, M., Hogg, C., & Hodgson, J. (2023). Nowcasting geoelectric fields in Ireland using magnetotelluric transfer functions. *Journal of Space Weather and Space Climate*, *13*, 6. https://doi.org/10.1051/swsc/2023004

Mann, I. R., Milling, D. K., Rae, I. J., Ozeke, L. G., Kale, A., Kale, Z. C., et al. (2008). The upgraded Carisma magnetometer array in the Themis era. *Space Science Reviews*, *141*(1–4), 413–451. https://doi.org/10.1007/s11214-008-9457-6

Marshalko, E., Kruglyakov, M., Kuvshinov, A., & Viljanen, A. (2023). Three-dimensional modeling of the ground electric field in fennoscandia during the Halloween geomagnetic storm. *Space Weather*, *21*(9), e2022SW003370. https://doi.org/10.1029/2022SW003370

Matzka, J., Bronkalla, O., da Silva, M. V., Kervalishvili, G., Rauberg, J., Korte, M., & Yamazaki, Y. (2024). Geomagnetic HPO index (V3.0) [Dataset]. *GFZ Data Services*. https://doi.org/10.5880/Hpo.0003

Matzka, J., Stolle, C., Yamazaki, Y., Bronkalla, O., & Morschhauser, A. (2021). The geomagnetic Kp index and derived indices of geomagnetic activity. *Space Weather*, *19*(5), e2020SW002641. https://doi.org/10.1029/2020SW002641

McLay, S. A., & Beggan, C. D. (2010). Interpolation of externally-caused magnetic fields over large sparse arrays using spherical elementary current systems. *Annales Geophysicae*, *28*(9), 1795–1805. https://doi.org/10.5194/angeo-28-1795-2010

McPherron, R., & Chu, X. (2017). The mid-latitude positive bay and the MPB index of substorm activity. *Space Science Reviews*, *206*(1–4), 91–122. https://doi.org/10.1007/s11214-016-0316-6

Menvielle, M., Papitashvili, N., Hakkinen, L., & Sucksdorff, C. (1995). Computer production of Kindices: Review and comparison of methods. *Geophysical Journal International*, *123*(3), 866–886. https://doi.org/10.1111/j.1365-246X.1995.tb06895.x

Morschhauser, A., Haseloff, J., Bronkalla, O., Müller-Brettschneider, C., & Matzka, J. (2017). A low-power data acquisition system for geomagnetic observatories and variometer stations. *Geoscientific Instrumentation, Methods and Data Systems*, *6*(2), 345–352. https://doi.org/10.5194/gi-6-345-2017

Obana, Y., Sakaguchi, K., Nosé, M., Hosokawa, K., Jaquiery, P., Saita, S., et al. (2024). New observational projects in New Zealand for studying radiation belt loss processes in the deep inner magnetosphere: Instrumentation, operation by solar power and initial results. *Earth Planets and Space*, *76*(1), 42. https://doi.org/10.1186/s40623-024-01990-0

Oliveira, D. M., Zesta, E., & Nandy, D. (2025). The 10 October 2024 geomagnetic storm may have caused the premature reentry of a Starlink satellite. *Frontiers in Astronomy and Space Sciences*, *11*, 1522139. https://doi.org/10.3389/fspas.2024.1522139

Oughton, E. J., Hapgood, M., Richardson, G. S., Beggan, C. D., Thomson, A. W. P., Gibbs, M., et al. (2019). A risk assessment framework for the socioeconomic impacts of electricity transmission infrastructure failure due to space weather: An application to the United Kingdom. *Risk Analysis*, *39*(5), 1022–1043. https://doi.org/10.1111/risa.13229

Parker, W. E., & Linares, R. (2024). Satellite drag analysis during the May 2024 Gannon geomagnetic storm. *Journal of Spacecraft and Rockets*, *61*(5), 1412–1416. https://doi.org/10.2514/1.A36164

Patterson, C., Wild, J., Beggan, C., Richardson, G. S., & Boteler, D. H. (2024). Modelling electrified railway signalling misoperations during extreme space weather events in the UK. *Scientific Reports*, *14*(1), 1583. https://doi.org/10.1038/s41598-024-51390-3

Pedersen, L. W., & Merenyi, L. (2016). The FGE magnetometer and the intermagnet 1 second standard. *Journal of Indian Geophysical Union*, *2*, 30–36.

Piersanti, M., Oliveira, D. M., D'Angelo, G., Diego, P., Napoletano, G., & Zesta, E. (2025). On the geoelectric field response to the SSC of the May 2024 super storm over Europe. *Space Weather*, *23*(2), e2024SW004191. https://doi.org/10.1029/2024SW004191

Pirjola, R. (2002). Review on the calculation of surface electric and magnetic fields and of geomagnetically induced currents in ground-based technological systems. *Surveys in Geophysics*, *23*(1), 71–90. https://doi.org/10.1023/A:1014816009303

Pratscher, K. M., Ingham, M., Mac Manus, D. H., Kruglyakov, M., Heise, W., Rodger, C. J., et al. (2024). Modeling GIC in the southern south island of aotearoa New Zealand using magnetotelluric data. *Space Weather*, *22*(7), e2024SW003907. https://doi.org/10.1029/2024SW003907

Pulkkinen, A., Viljanen, A., Pajunpää, K., & Pirjola, R. (2001). Recordings and occurrence of geomagnetically induced currents in the Finnish natural gas pipeline network. *Journal of Applied Geophysics*, *48*(4), 219–231. https://doi.org/10.1016/S0926-9851(01)00108-2

Riddick, J., & Stuart, W. (1984). The generation of k indices from digitally recorded magnetic data. *Geophysical Surveys*, *6*(3–4), 439–456. https://doi.org/10.1007/BF01465559

Rodger, C. J., Clilverd, M. A., Mac Manus, D. H., Martin, I., Dalzell, M., Brundell, J. B., et al. (2020). Geomagnetically induced currents and harmonic distortion: Storm-time observations from New Zealand. *Space Weather*, *18*(3), e2019SW002387. https://doi.org/10.1029/2019SW002387

Rodger, C. J., Mac Manus, D. H., Dalzell, M., Thomson, A. W. P., Clarke, E., Petersen, T., et al. (2017). Long-term geomagnetically induced current observations from New Zealand: Peak current estimates for extreme geomagnetic storms. *Space Weather*, *15*(11), 1447–1460. https://doi.org/10.1002/2017SW001691

Rogers, N. C., Wild, J. A., Eastoe, E. F., Gjerloev, J. W., & Thomson, A. W. (2020). A global climatological model of extreme geomagnetic field fluctuations. *Journal of Space Weather and Space Climate*, *10*, 5. https://doi.org/10.1051/swsc/2020008

Rosenqvist, L., Johlander, A., Molenkamp, S., Dimmock, A. P., Setréus, J., & Lanabere, V. (2025). A novel approach for evaluating GIC impacts in the Swedish power grid. *Space Weather*, *23*(6), e2024SW004313. https://doi.org/10.1029/2024SW004313

Rostoker, G. (1972). Geomagnetic indices. *Reviews of Geophysics*, *10*(4), 935–950. https://doi.org/10.1029/rg010i004p00935

Schmidt, A., Dabas, M., & Sarris, A. (2020). Dreaming of perfect data: Characterizing noise in archaeo-geophysical measurements. *Geosciences*, *10*(10), 382. https://doi.org/10.3390/geosciences10100382

Shao, Q., Liu, Y., Luo, Y., Heinson, G., Xu, Y., Du, J., & Chen, C. (2024). Geoelectric field estimations during geomagnetic storm in north China from sinoprobe magnetotelluric impedances. *Space Weather*, *22*(4), e2023SW003758. https://doi.org/10.1029/2023SW003758

Shiokawa, K., Nomura, R., Sakaguchi, K., Otsuka, Y., Hamaguchi, Y., Satoh, M., et al. (2010). The STEL induction magnetometer network for observation of high-frequency geomagnetic pulsations. *Earth Planets and Space*, *62*(6), 517–524. https://doi.org/10.5047/eps.2010.05.003

Silverman, S., & Cliver, E. (2001). Low-latitude auroras: The magnetic storm of 14–15 May 1921. *Journal of Atmospheric and Solar-Terrestrial Physics*, *63*(5), 523–535. https://doi.org/10.1016/S1364-6826(00)00174-7

Skey, H. (1921). The recent magnetic storm, 14th to 17th May, 1921. *New Zealand Journal of Science and Technology*, *4*, 197–201.

Smith, A. W., Freeman, M. P., Rae, I. J., & Forsyth, C. (2019). The influence of sudden commencements on the rate of change of the surface horizontal magnetic field in the United Kingdom. *Space Weather*, *17*(11), 1605–1617. https://doi.org/10.1029/2019SW002281

Smith, A. W., Rodger, C. J., Mac Manus, D. H., Rae, I. J., Fogg, A. R., Forsyth, C., et al. (2024). Sudden commencements and geomagnetically induced currents in New Zealand: Correlations and dependence. *Space Weather*, *22*(1), e2023SW003731. https://doi.org/10.1029/2023SW003731

St-Louis, B. (2024). *Intermagnet technical reference manual, version 5.1. 1*. INTERMAGNET Operations Committee and Executive Council.

Tanskanen, E. (2009). A comprehensive high-throughput analysis of substorms observed by image magnetometer network: Years 1993–2003 examined. *Journal of Geophysical Research*, *114*(A5). https://doi.org/10.1029/2008JA013682

Thomson, A. W., Dawson, E. B., & Reay, S. J. (2011). Quantifying extreme behavior in geomagnetic activity. *Space Weather*, *9*(10). https://doi.org/10.1029/2011sw000696

Tikhonov, A. (1950). On determining electrical characteristics of the deep layers of the Earth's crust. *Doklady*, *73*, 295–297.

Trichtchenko, L. (2021). Frequency considerations in GIC applications. *Space Weather*, *19*(8), e2020SW002694. https://doi.org/10.1029/2020SW002694

Tsurutani, B. T., Hajra, R., Echer, E., & Gjerloev, J. W. (2015). Extremely intense (SML≤ −2500 nT) substorms: Isolated events that are externally triggered? *Annales Geophysicae*, *33*(5), 519–524. https://doi.org/10.5194/angeo-33-519-2015

United Nations. (2017). *Report on thematic priority 4: International framework for space weather services for unispace+ 50 (a/ac. 105/1171)*. Author. Retrieved from https://www.unoosa.org/oosa/oosadoc/data/documents/2018/aac.105/aac.1051171_0.html

Viljanen, A. (1998). Relation of geomagnetically induced currents and local geomagnetic variations. *IEEE Transactions on Power Delivery*, *13*(4), 1285–1290. https://doi.org/10.1109/61.714497

Viljanen, A., Nevanlinna, H., Pajunpää, K., & Pulkkinen, A. (2001). Time derivative of the horizontal geomagnetic field as an activity indicator. *Annales Geophysicae*, *19*(9), 1107–1118. https://doi.org/10.5194/angeo-19-1107-2001

Weygand, J. M., Zesta, E., & Troshichev, O. (2014). Auroral electrojet indices in the northern and southern hemispheres: A statistical comparison. *Journal of Geophysical Research: Space Physics*, *119*(6), 4819–4840. https://doi.org/10.1002/2013JA019377

Weygand, J. M., Zhelavskaya, I., & Shprits, Y. (2021). A comparison of the location of the mid-latitude trough and plasmapause boundary. *Journal of Geophysical Research: Space Physics*, *126*(4), e2020JA028213. https://doi.org/10.1029/2020JA028213

Wik, M., Pirjola, R., Lundstedt, H., Viljanen, A., Wintoft, P., & Pulkkinen, A. (2009). Space weather events in July 1982 and October 2003 and the effects of geomagnetically induced currents on Swedish technical systems. *Annales Geophysicae*, *27*(4), 1775–1787. https://doi.org/10.5194/angeo-27-1775-2009

Yamazaki, Y., Matzka, J., Stolle, C., Kervalishvili, G., Rauberg, J., Bronkalla, O., et al. (2022). Geomagnetic activity index HPO. *Geophysical Research Letters*, *49*(10), e2022GL098860. https://doi.org/10.1029/2022GL098860

Zou, Y., Ohtani, S., Gjerloev, J. W., Anderson, B. J., Waters, C. L., Wang, C.-P., et al. (2025). Are supersubstorms substorms? Extreme nightside auroral electrojet activities during the May 2024 geomagnetic storm. *Journal of Geophysical Research: Space Physics*, *130*(3), e2024JA033303. https://doi.org/10.1029/2024JA033303